

ABE-VVS: Attribute-Based Encrypted Volumetric Video Streaming

Mohammad Waquas Usmani

mohammadwaqu@umass.edu

University of Massachusetts Amherst

Massachusetts, USA

Susmit Shannigrahi

sshannigrahi@tnitech.edu

Tennessee Technological University

Tennessee, USA

Michael Zink

zink@ecs.umass.edu

University of Massachusetts Amherst

Massachusetts, USA

Abstract

This work introduces ABE-VVS, a framework that performs attribute based selective coordinate encryption for point cloud based volumetric video streaming, enabling lightweight yet effective digital rights management (DRM). Rather than encrypting entire point cloud frames, our approach encrypts only selected subsets of coordinates (X , Y , Z , or combinations), lowering computational overhead and latency while still producing strong visual distortion that prevents meaningful unauthorized viewing. Our experiments show that encrypting only the X coordinates achieves effective obfuscation while reducing encryption and decryption times by up to 50% and 80%, respectively, compared to full-frame encryption.

To our knowledge, this is the first work to provide a novel end-to-end evaluation of a DRM-enabled secure point cloud streaming system. We deployed a point cloud video streaming setup on the CloudLab testbed and evaluated three HTTP-based Attribute-Based Encryption (ABE) granularities – ABE-XYZ (encrypting all X , Y , Z coordinates), ABE-XY, and ABE-X—against conventional HTTPS/TLS secure streaming as well as an HTTP-only baseline without any security. Our streaming evaluation demonstrates that ABE-based schemes reduce server-side CPU load by up to 80% and cache CPU load by up to 63%, comparable to HTTP-only, while maintaining similar cache hit rates. Moreover, ABE-XYZ and ABE-XY exhibit lower client-side rebuffering than HTTPS, and ABE-X achieves zero rebuffering comparable to HTTP-only. Although ABE-VVS increases client-side CPU usage, the overhead is not large enough to affect streaming quality and is offset by its broader benefits, including simplified key revocation, elimination of per-client encryption, and reduced server and cache load.

Keywords

Point Clouds, Volumetric Video, 6DoF, Streaming, Attribute-Based Encryption, Selective Encryption, Digital Rights Management

1 Introduction

Augmented and Virtual Reality (AR/VR) are rapidly emerging as major trends in next-generation multimedia, offering levels of immersion far beyond conventional formats. Unlike traditional 2D or 360° videos [16, 42], which restrict the viewer to three degrees of freedom (3DoF) and permit only rotational movement from a fixed position, volumetric AR/VR content enables six degrees of freedom (6DoF) [7, 11, 18, 37]. This allows users both to view in any direction and to move naturally within a virtual environment.

A key data representation powering these immersive experiences is the point cloud [7, 11, 18]. Point clouds describe 3D scenes using collections of points, each storing geometric coordinates (x, y, z) and appearance attributes such as color (r, g, b). Complex environments are constructed by assembling multiple 3D objects into a single point cloud frame. When these frames are played in

sequence, they form a volumetric video [7, 11, 18, 37] typically viewed through head-mounted displays (HMDs).

However, delivering such immersive content introduces several challenges. Point clouds contain substantially more data than traditional video formats, leading to high computational requirements and the demand for high streaming bitrates. These demands can increase end-to-end latency, which is particularly problematic for immersive applications that rely on very low delay to maintain responsiveness [7]. Elevated latency contributes directly to motion-to-photon delay [10], a major factor in cybersickness and a significant barrier in immersive experience [35]. In addition, securing volumetric streams—through digital rights management (DRM), fine-grained access control, and protected distribution—adds yet another layer of computational overhead, making it even more difficult to meet stringent latency requirements.

While considerable research has advanced volumetric content streaming on head-mounted displays—ranging from improving quality of experience (QoE) through viewport prediction [10, 27] and adaptive quality streaming [45] to progress in point cloud compression and encoding [21, 28]—there has also been notable development of end-to-end volumetric video delivery systems designed for scalability and low latency [7, 10, 11]. Several efforts integrate DASH [34] into volumetric streaming pipelines [6, 12, 13, 45], and others incorporate machine-learning-based super-resolution [47] to improve rendered quality.

In contrast, secure distribution and access control for volumetric video have seen far less attention [37]. Most existing security mechanisms target isolated point cloud objects [1, 14, 17, 19, 20] rather than continuous volumetric video streams, leaving a significant gap in scalable DRM solutions for immersive media.

In this paper, we present Attribute-Based Encrypted Volumetric Video Streaming (ABE-VVS), a framework that applies attribute-based selective point-cloud encryption to balance security with low computational overhead tailored specifically for volumetric streaming. ABE-VVS allows encrypting coordinates within point cloud frames at varying levels. By encrypting only the targeted coordinates, ABE-VVS degrades and distorts the visual quality that prevents meaningful viewing by unauthorized users. Built on Attribute-Based Encryption (ABE)[4], ABE-VVS secures the content itself—both in transit and at rest—eliminating the need for separate transport-layer protection, consistent with prior work [41, 42]. To the best of our knowledge, ABE-VVS is the first complete, DRM-enabled secure volumetric point-cloud streaming system.

Within the ABE-VVS framework, The origin encrypts each point cloud using attribute policies, enabling the content to be cached or distributed from any location. Upon receiving the encrypted content, the client requests a decryption key from the license server, which issues a key containing the necessary attributes that enables client to perform decryption. Time-based attributes can also be used

to enforce automatic key expiration that revokes access without the need to re-encrypt the content.

We evaluate ABE-VVS's potential within a secure volumetric point cloud streaming system by testing multiple encryption granularities and comparing performance against conventional HTTPS-based secure streaming as well as unsecured HTTP-only streaming. Our results demonstrate that ABE-VVS reduces server CPU usage by up to 80% and reduces cache CPU load by up to 63% achieving similar efficiencies with unsecured HTTP-only streaming while preserving similar cache hit rates and rebuffering-free client side playback.

2 Background and Related Work

This section provides an overview of 3D point clouds, Attribute-Based Encryption, and recent work on point cloud encryption and point cloud streaming.

2.1 3D Point Clouds

Point clouds are composed of discrete 3D points, each represented by spatial coordinates (x, y, z) and, in many cases, additional attributes such as color (r, g, b) or surface normals (n_x, n_y, n_z) . These points collectively describe the geometry of an object or scene and are commonly stored as individual frames in the standard polygon file format (.PLY) [38]. Unlike conventional image or video data, point clouds provide a flexible, spatially detailed representation. When such frames are captured sequentially, they form a volumetric video, enabling full six degrees of freedom (6DoF) interaction for the user [37], compared to the three degrees of freedom available in 360-degree video experiences [42].

2.2 Point Cloud Security

A variety of studies have explored security mechanisms for point clouds. Several approaches, such as [1, 17, 20], rely on chaotic-map-based transformations, while others, including [19], use permutation and geometric rotation for encryption. More recent methods [1, 19, 20] emphasize on preserving dimensional or spatial consistency—ensuring that an object's scale, proportions, and overall structure remain intact—so that encrypted point clouds can coexist with unencrypted elements inside virtual environments. Despite these advances, most existing techniques target full object-level protection for standalone point clouds, offering strong cryptographic security but often incurring significant computational cost.

For instance, decrypting a 100k-point cloud requires 8–9 seconds in [19], 4–5 seconds in [1], and roughly 30 ms for 40k points in [17] (which scales to approximately 75 ms for 100k points). Since decryption occurs on the user side—often on resource-constrained VR and AR headsets, these costs directly impact playback latency. In comparison, our method decrypts a 108k-point cloud in only 45 ms, even when all X , Y , and Z coordinates are processed. This represents a substantial computational improvement and makes our approach suitable for the low-latency requirements of volumetric video streaming, where 15–30 point cloud frames must be processed each second.

Unlike [14], which uses ABE and watermarking to manage access and trace misuse in isolated 3D models—without examining the time cost of encryption or decryption—our work focuses on volumetric

video, providing low-latency encryption and practical DRM across continuous point cloud frames.

VVSec [37] protects volumetric video by introducing adversarial perturbations that distort 3D face geometry and prevent misuse in deep-learning pipelines. This defense, however, is non-reversible—legitimate users cannot reconstruct the original model—and producing the perturbations is costly, requiring 3–9 seconds per frame. By contrast, our method supports full restoration by authorized viewers rather than applying permanent obfuscation.

2.3 Point Cloud Video Streaming

Hosseini and Timmerer introduced DASH-PC [13], the first system to adapt MPEG-DASH for dynamic point cloud streaming of a single point-cloud object, enabling adaptive, per-frame streaming. They generate multiple Level-of-Density (LoD) representations through density sub-sampling and describe these in an MPD-like manifest, allowing clients to switch quality levels based on bandwidth, similar to traditional ABR streaming.

Van der Hooft et al. introduced PCC-DASH [45], highlighting and addressing the limitations of DASH-PC's frame-based and single-object design. Their system uses segment-based streaming for multi-object volumetric scenes, with each object represented as a DASH AdaptationSet in the MPD and annotated with its position in the 3D scene. They further employ MPEG V-PCC compression to create multiple bitrate/quality levels, and introduce additional rate-adaptation mechanisms based on the user's 6DoF position and viewport, determining which objects to fetch and at what quality. They later conducted subjective and objective QoE evaluations of PCC-DASH in [44].

More recently, Chujo et al. [6] proposed a perceptual-quality-driven DASH streaming approach for point clouds. Orthogonal to DASH-centric efforts, Zhang et al. introduced YuZu [47], which incorporates super-resolution into the volumetric video pipeline: the system streams downsampled versions to save bandwidth and performs client-side upsampling using an ML-based super-resolution model, effectively acting as an SR-aware volumetric ABR system with demonstrated QoE gains. Most recently, Heidarirad and Wang introduced VV-DASH [12], an end-to-end, codec-agnostic DASH framework for volumetric video. In addition, Liu et al. [22] proposed using client-side caching to buffer repeated tiles in volumetric video streams to eliminate redundant network transfers.

None of these systems considers securing the streaming pipeline or providing any form of DRM. By contrast, our work explicitly introduces encryption into the volumetric streaming pipeline. ABE-VVS performs frame-based streaming of point clouds, without any compression, viewport adaptation, or other performance optimizations, creating a worst-case streaming scenario. This allows us to isolate and quantify the impact of introducing a selective attribute-based encryption layer on end-to-end latency, cacheability, and QoE. The optimization techniques developed in prior works are orthogonal to our approach and can be integrated into our pipeline to further improve efficiency. To the best of our knowledge, we are the first to treat encryption as a first-class component of a volumetric streaming system.

2.4 Distributed & Secure Point Cloud Streaming

While our streaming client currently uses a single-bitrate configuration and performs frame-based delivery, ABE-VVS is fully compatible with the volumetric DASH-ABR techniques described in Sect. 2.3, and such optimizations can be readily integrated into our pipeline to further improve efficiency and adaptivity.

HTTP Secure (HTTPS) extends HTTP by encrypting communication using TLS [33], where a short-term session key is negotiated through long-term public and private keys to secure data exchange. A key limitation of HTTPS is its host-centric, point-to-point design: content must be encrypted separately for each receiver, increasing computational load on servers and reducing the effectiveness of caching, as we will demonstrate in the evaluation of ABE-VVS.

Content Distribution Networks (CDN) improves large-scale media delivery by caching and serving content from geographically distributed edge nodes. This reduces latency, lowers origin-server load, and provides more stable performance during periods of high demand. While originally designed for conventional video, the same infrastructure can support volumetric point cloud video distribution: each point cloud frame can be cached and delivered as an independent object. Caching can be potentially improved by tailoring admission and eviction algorithms to the characteristics of point clouds, but such work is beyond the scope of this paper.

Caching for plain HTTP is simple because intermediaries can store and forward content directly. However, HTTPS complicates caching since CDN nodes must perform TLS/SSL termination [46]. When a client makes a request, the CDN negotiates a secure channel, checks if the requested content is cached, and—if it is missing or stale—retrieves it securely from the origin server. Before serving it to the client, the CDN must re-encrypt the content and create a fresh TLS session [39, 46]. This involves decrypting and re-encrypting data at every hop, which adds noticeable computational overhead.

2.5 Attribute-Based Encryption (ABE):

Attribute-Based Encryption (ABE) is a public-key cryptographic approach that supports fine-grained, scalable access control. Rather than relying on explicit user identities, ABE issues keys and enforces access rules based on descriptive attributes such as a user's role, affiliation, or region. In ABE, each ciphertext includes an access policy Q , and users obtain private keys annotated with their attribute sets. Decryption is possible only when the user's attributes satisfy the embedded policy. *This design enables adaptable key management, allowing attributes and user keys to be modified or revoked without re-encrypting the underlying data.*

2.5.1 Access Control Policy: Consider a VR data-sharing platform that needs to regulate access to immersive 3D content.

(a) Example Policy: Access is granted only to users who have the Researcher role and who are either affiliated with University X or located in Asia.

(b) User Attributes: Each user is issued a private key SK containing their attribute set. For instance, **Alice** holds **{Role: Researcher, Affiliation: UnivX}**, whereas **Bob** has **{Role: Student, Region: Asia}**.

(c) Encryption and Decryption: The content provider encrypts the VR dataset under public key PK with the policy: “**Role = Researcher AND (Affiliation = UnivX OR Region = Europe)**.” Only

users whose attributes satisfy this rule—such as Alice—are able to decrypt the dataset.

2.5.2 Key Revocation and Updates: One advantage of ABE is its ability to handle revocation and attribute changes without re-encrypting stored data. For example, if Alice leaves the research group, her key SK can be revoked or assigned an expiration time. Time-based revocation is commonly implemented by adding an expiration attribute to user keys, as demonstrated in [29, 31, 32]. Administrators can periodically refresh or invalidate these attributes as required.

By embedding access policies directly into the encrypted content, ABE enables the efficient management of user onboarding, role transitions, and regional restrictions through key updates, rather than costly data re-encryption, making it a strong fit for distributed VR and 3D point cloud content platforms.

2.6 ABE for Streaming:

Prior work [25, 41, 42] has applied ABE to video streaming, focusing mainly on traditional 2D and 360° content. Studies such as [41, 42] demonstrate that using ABE over HTTP can lower cache CPU load while preserving QoE when compared to HTTPS. Although [42] also explores frame-level selective encryption, these techniques are designed for the structure of compressed video streams and do not translate to point cloud formats.

Prior work [40] introduced a novel attribute-based selective coordinate encryption technique for point cloud data, whose representation and encoding differ fundamentally from traditional video formats and their corresponding encryption methods. Unlike prior ABE-based approaches, this approach operates directly on the spatial geometry of point clouds by encrypting selected X, Y, Z coordinates, enabling a fine-grained and flexible encryption granularity. Building on this foundation, [43] extends the approach with point cloud frame downsampling to reduce bandwidth and latency, and using machine-learning-based super-resolution to reconstruct high-quality content at the client. The present work is different as it evaluates ABE-VVS in a full end-to-end volumetric streaming scenario, including its potential to offer ABE-enabled caching benefits—such as reducing computational load at intermediate caches.

3 System Architecture

In this section, we describe the overall system architecture of ABE-VVS and outline the key design choices behind its major components. Figure 1 shows a simplified representation of such point cloud video distribution pipeline, highlighting the core elements relevant to our framework.

3.1 HTTP-Based Point Cloud Streaming

Most large-scale video platforms rely on CDNs and DASH/HLS-style ABR delivery. Our goal is to develop a volumetric point cloud streaming system that naturally fits within this ecosystem while supporting attribute-based selective coordinate encryption. To this end, we build a DASH-like player that parses an MPD, downloads frames via HTTP, HTTPS, or our HTTP-ABE mode, and maintains a playback buffer. Although our current prototype operates at a single quality level for evaluation purposes, the design is compatible with future ABR extensions.

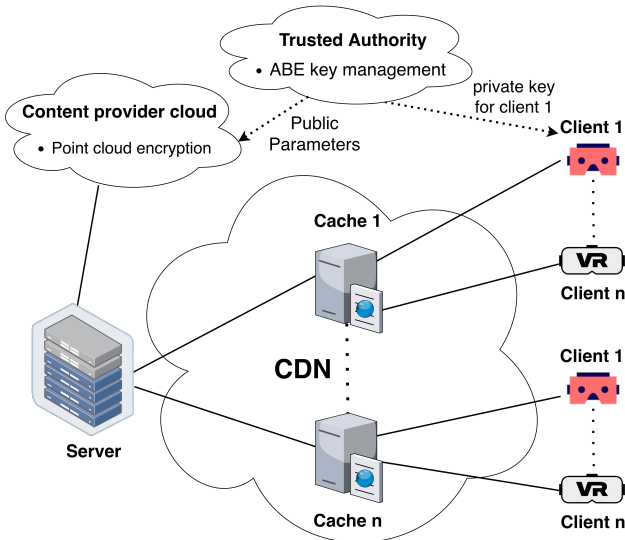


Figure 1: System Architecture

Our approach introduces a selective encryption mechanism tailored to volumetric content (Sect. 3.2). Unlike conventional HTTP-based delivery, where content is either fully encrypted (HTTPS) or entirely unencrypted (HTTP), we encrypt only targeted coordinates within each point cloud frame. To signal these encrypted components, we extend the MPD with an “*encryption level*” attribute that specifies which coordinate subsets were protected. The client-side player reads this metadata and performs the correct selective ABE decryption scheme and re-constructs the point cloud frame.

A second requirement is secure key distribution. In contrast to HTTPS, where TLS implicitly handles key exchange, our system relies on a Trusted Authority (TA) that issues ABE keys to both the content provider and authorized clients. Caches remain oblivious: they store and serve encrypted point clouds without performing any cryptographic operations or participating in key management.

We discuss the ABE-VVS prototype used in our evaluation in Sect. 3.3.

3.2 Selective Coordinate Encryption of Point Clouds

Figure 2 illustrates the overall workflow of our selective-coordinate encryption pipeline.

Our goal is to reduce computational cost by encrypting only a subset of point cloud coordinates. *Rather than aiming for complete privacy, we target substantial visual obfuscation and distortion that prevents meaningful unauthorized viewing.* To support flexible, per-coordinate encryption, we extend the CPABE [4] toolkit with the ability to parse binary PLY files and selectively operate on individual coordinate fields. Although our current implementation is tailored to the PLY format, the same mechanism can be applied to other point cloud representations.

Algorithm 1 summarizes the process, which takes as input the public key PK , a policy Q , and a user-defined pattern P describing

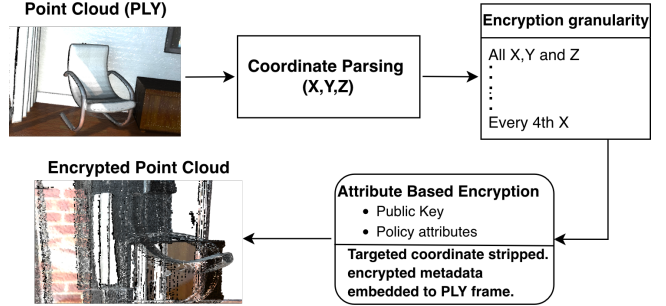


Figure 2: Selective Coordinate Encryption Process

the desired encryption granularity. The *pattern P* specifies which coordinates are selectively encrypted. For example, XYZ encrypts all X, Y, Z coordinates, while 2XY encrypts every second X coordinate and all Y coordinates. Other combinations are also possible, providing a flexible and fine-grained mechanism to explore security, size, and quality trade-offs under selective encryption. The targeted coordinates are collected from each vertex into a buffer, and their original values are removed from the vertex data. This buffer is then encrypted using ABE and appended to the PLY frame in combination with an encryption marker to produce the encrypted output. All remaining elements—such as normals, colors, and the PLY header—are left unchanged.

Algorithm 1 Selective Coordinate Encryption for Point Clouds

Input: PLY file F_{in} , pattern P , public key PK , policy Q
Output: Encrypted file F_{out} , encrypted buffer C^*

```

1: Read header from  $F_{in}$  and obtain number of vertices  $N$ 
2: Initialize buffer  $C \leftarrow \emptyset$ 
3: for  $n = 0$  to  $N - 1$  do
4:   Read vertex  $v_n$  from  $F_{in}$ 
5:   Initialize removed vertex  $v'_n \leftarrow \text{empty}$ 
6:   for all coordinate  $d \in \{x, y, z\}$  do
7:     if  $d$  is targeted by pattern  $P$  at index  $n$  then
8:       Append original value  $v_n.d$  to  $C$ 
9:       remove key  $d$  from  $v'_n$             $\triangleright$  Removed coordinate
10:    else
11:      set  $v'_n[d] \leftarrow v_n.d$             $\triangleright$  Keep coordinate
12:    end if
13:   end for
14:   Copy all non-coordinate attributes (colors, normals, etc.) into  $v'_n$ 
15:   Write  $v'_n$  to  $F_{out}$ 
16: end for
17: Encrypt buffer  $C$  using  $PK$  and  $Q$  to produce  $C^*$ 
18: Append encryption marker and  $C^*$  to  $F_{out}$ 

```

Algorithm 2 describes how authorized clients reconstruct the original point cloud frame. After locating and decrypting the encrypted buffer, the client reinserts the removed coordinate values into their respective positions, as determined by the same granularity pattern P , thereby fully restoring the original 3D frame.

Algorithm 2 Selective Coordinate Decryption and Restoration

Input: Encrypted file F_{enc} , pattern P , private key SK
Output: Restored PLY file F_{dec}

```

1: Read header from  $F_{enc}$  and get number of vertices  $N$ 
2: Locate marker, extract encrypted buffer  $C^*$ 
3: Decrypt  $C^*$  with  $SK$  to obtain plaintext buffer  $C$ 
4:  $i \leftarrow 0$ 
5: for  $n = 0$  to  $N - 1$  do
6:   Read removed vertex  $v_n$  from  $F_{enc}$ 
7:   Initialize restored vertex  $v_n^R \leftarrow v_n$ 
8:   for all coordinate  $d \in \{x, y, z\}$  do
9:     if  $d$  is targeted by pattern  $P$  at index  $n$  then
10:      set  $v_n^R[d] \leftarrow C[i]$     $\triangleright$  Restore removed coordinate
11:       $i \leftarrow i + 1$ 
12:    else
13:      retain  $v_n[d]$  in  $v_n^R$     $\triangleright$  Coordinate wasn't removed
14:    end if
15:   end for
16:   Write  $v_n^R$  to  $F_{dec}$ 
17: end for

```

Assuming that an unauthorized viewer could attempt to fill missing coordinates with zeros to render the point cloud frame, we also evaluated a “zeroed-coordinate” variant in which targeted coordinates are preserved as zeros rather than removed. This variant is used solely to quantify the level of visual obfuscation achieved under different encryption granularities. The corresponding results of our selective encryption for point clouds are presented in Sect. 4.1.4.

3.3 Prototype Implementation

In this section, we present the implemented prototype of ABE-VVS using the following components:

3.3.1 Ciphertext-Policy Attribute-Based Encryption Toolkit: We implement ABE using the CPABE toolkit [4], which follows the scheme introduced in [5]. The setup phase produces a master key (MK) and a public key (PK). The PK is used to encrypt data under an access policy Q that specifies the attribute conditions required for decryption. User keys (SK) are generated from the master key and the public key, and each SK is associated with a set of attributes. Decryption succeeds only when the attributes encoded in the user’s SK satisfy the policy Q embedded in the ciphertext. As detailed in Sect. 3.2, we extend the CPABE toolkit to support selective coordinate encryption and decryption of point cloud frames.

3.3.2 PC-Stream client: We implemented a lightweight, per-frame point cloud streaming client *PC-Stream* inspired by prior work [13]. *PC-Stream* accepts an MPD file ($-URL$) and parses it to obtain frame rate, per-frame point cloud URLs, and the encryption level indicating the coordinate granularity used during encryption. Both HTTP and HTTPS are supported, as identified by the MPD URL scheme.

The client maintains a configurable playback buffer ($-buffer$), expressed in seconds. For example, a value of 2 permits up to two seconds’ worth of frames to be queued; if full, the client polls every

1ms for available space. This buffer also serves as the initial startup buffer before playback begins.

We integrate our attribute-based selective coordinate decryption module directly into the client. Decryption can be enabled via $-decrypt$, supplying the public key ($-pub$) and user private key ($-priv$). An optional $-download-queue$ parameter enables parallel decryption and downloading, allowing up to a specified number of frames to be fetched while earlier frames are still being decrypted. This feature is only applicable to the ABE workflow, since HTTPS already benefits from parallel cryptographic processing within the TLS pipeline. By default, all downloading and decryption are performed entirely in memory, avoiding disk writes and eliminating unnecessary I/O overhead.

Using PC-Stream, we compare three delivery modes: HTTP (no security), HTTP-ABE (selective coordinate decryption enabled), and HTTPS (via an <https://> MPD URL).

In addition to streaming and decryption, PC-Stream also performs detailed runtime logging. For each frame, the client records download time, decryption time, and the timestamped progression of playback events—including the current frame index, buffer occupancy, and buffer fill/empty transitions—to enable fine-grained analysis. PC-Stream also detects and logs stalls, capturing both the start time and duration whenever playback pauses due to an empty buffer. These logs allow us to compute end-to-end streaming performance QoE metrics, such as rebuffering.

Note that PC-Stream operates at the granularity of individual frames, representing a worst-case scenario where the number of GET requests equals the frame rate. Recent systems mitigate this cost using segment-based delivery, point cloud compression, and viewport adaptation (Sect. 2.3). Our design isolates the effect of introducing an ABE layer on end-to-end performance, cacheability, and QoE. Optimizations in prior works are orthogonal to our contribution and can be incorporated in future work.

4 Evaluation

In this section, we first evaluate the performance of our selective coordinate encryption approach, and then compare the performance of ABE-VVS in point cloud video streaming against HTTPS and HTTP-only.

4.1 Impact of Selective Coordinate Encryption under ABE

We evaluate the performance of our selective coordinate encryption on a node from CloudLab [9] testbed. The same CloudLab cluster was later used in our streaming evaluation to maintain consistency.

4.1.1 Point Cloud Dataset: We use five point clouds from the datasets provided by Open3D [26] in PLY format that were acquired from RGB-D captures. Each point cloud includes per-point geometric and appearance attributes: spatial coordinates (x, y, z), surface normals (n_x, n_y, n_z), and color values (r, g, b).

Coordinates and normals are stored as double-precision floating-point numbers (8 bytes each), whereas color channels are represented as unsigned 1-byte integers.

The point clouds used in our experiments are:

- **108k:** 108,161 points, from the Office dataset.

- **196k:** 196,133 points, from the Living Room dataset.
- **334k:** 334,736 points, from the Office dataset.
- **433k:** 433,393 points, from the Office dataset.
- **515k:** 515,284 points, from the Living Room dataset.

This offers a diverse range of resolutions (points per cloud) and scenes for comparative evaluation. Visual examples of the 108k, 334k, 433k, and 515k point clouds are shown in Fig. 3, while the 196k-point cloud is illustrated in Fig. 6a.



Figure 3: Visuals of four point clouds: 108k, 334k, 433k, 515k.

4.1.2 Quality Evaluation Metrics: To evaluate the geometric differences between original and modified point clouds, we use spatial metrics that directly measure discrepancies in 3D space and are standard in point cloud analysis. In our setting, these metrics also indicate how effectively the encryption or obfuscation alters the spatial structure. We compute them on the zeroed-coordinate version of our method, as detailed in Sect. 3.2, where targeted coordinates are replaced with zeros rather than removed.

Chamfer Distance (CD) [23, 36]: Chamfer Distance computes the average nearest-neighbor distance between two point clouds in both directions. For every point in one cloud, the closest point in the other is identified, and the distances are averaged in both forward and reverse mappings. While lower CD values typically indicate high geometric similarity in reconstruction settings, *in our context, larger CD values correspond to stronger obfuscation and greater deviation from the original geometry.*

Hausdorff Distance (HD) [15, 19]: Hausdorff Distance measures the maximum nearest-neighbor deviation between the two point sets, capturing worst-case geometric differences and remaining sensitive to outliers. As with CD, *higher HD values are preferable in our scenario, as they reflect increased geometric distortion and thus more effective obfuscation.*

4.1.3 Runtime evaluation: We evaluate the computational costs of ABE encryption and decryption across different selective coordinate granularities. The granularities examined include: **Full**—encrypting the entire frame without selection, used as our baseline; **XYZ**—encrypting all X , Y , Z coordinates; **XY**—encrypting only X and Y ; **X**—encrypting all X coordinates; and patterns that encrypt every n th X coordinate such as **2X**, **3X**, etc. This setup allows us to systematically study the trade-off between obfuscation and computational cost at different levels of encryption granularity. Although we present results for patterns such as XY and every n th X , similar behavior is expected for YZ or XZ, or for encrypting every n th Y or Z ; therefore, we do not exhaustively evaluate all permutations.

For clarity, we use a single-attribute ABE policy in these experiments. Streaming deployments may require up to five attributes, but prior work [30] shows that encryption time scales linearly with

the number of attributes, and increasing from one to five adds negligible overhead.

Encryption Runtime: For each point cloud, we executed 1000 runs per granularity and recorded the encryption times. Figure 4a reports runtimes in milliseconds, while Fig. 4b shows percentage reductions compared to full-frame encryption (baseline with no selective encryption). The XYZ granularity yields up to a 22% reduction, whereas XY achieves up to 37%, and encrypting only X results in 40–50% savings across the datasets. Coarser granularities such as 2X–5X exhibit similar reductions (40–50%) as X. This is because fixed ABE overheads dominate, particularly for smaller point clouds such as 108k, where further reducing the encrypted data size has diminishing impact. Figure 4c illustrates that encryption time scales nearly linearly with point cloud size for the X granularity.

Decryption Runtime: For each granularity, we repeat the decryption process 1000 times and report the average runtime. Figure 5a reports runtimes in milliseconds, and Fig. 5b shows the percentage of savings compared to the baseline full-frame decryption. Similar to encryption, coarser granularities reduce computation. We observe reductions of up to 58% for XYZ, 70% for XY, and 74–82% for X. Coarser granularities such as 2X–5X provide reductions comparable to X, with improvements plateauing due to fixed ABE and parsing overheads.

Notably, decryption achieves substantially larger reductions than encryption. This is partly because full-frame decryption is more expensive (e.g., 443 ms for 515k) than full-frame encryption (311 ms for 515k). Nevertheless, across all selective coordinate granularities (XYZ, XY, etc), decryption remains faster than encryption. Figure 5c shows that decryption time scales nearly linearly with point cloud size under the X scheme, but consistently takes roughly half the time required for encryption (Fig. 4c). This asymmetry is advantageous in practice: decryption occurs on client devices—often resource-constrained VR/AR headsets—where minimizing latency is critical. Conversely, encryption is performed by content providers with significantly more compute capacity.

Size overhead: We also evaluated the ABE metadata overhead and found that it adds a negligible increase in size across all encryption granularities. On average, the encrypted buffer adds only about 580 bytes per point cloud—amounting to roughly 0.01% for a 108k-point cloud and 0.002% for a 515k-point cloud. This small and consistent overhead results from using a single-attribute ABE policy, whose size scales linearly with the number of attributes [30], consistent with observations in prior work [41]. Such a minimal increase is unlikely to impact streaming performance.

4.1.4 Impact of Zeroed Coordinates: Here we aim to evaluate the amount of obfuscation provided by different encryption granularities by applying the quantitative spatial metrics from Sect. 4.1.2. As detailed in Sect. 3.2, our streaming design removes the targeted coordinate entirely. However, in a worst-case scenario for security, any unauthorized person could potentially find the removed coordinate positions and replace them with zeros, producing a syntactically valid but geometrically and visually distorted PLY frame. Our analysis measures the similarity between these “zero-filled” reconstructions and the original to evaluate the level of obfuscation.

Figure 6 visualizes the 196k-point cloud under several granularities with the targeted coordinates zeroed; the original is shown

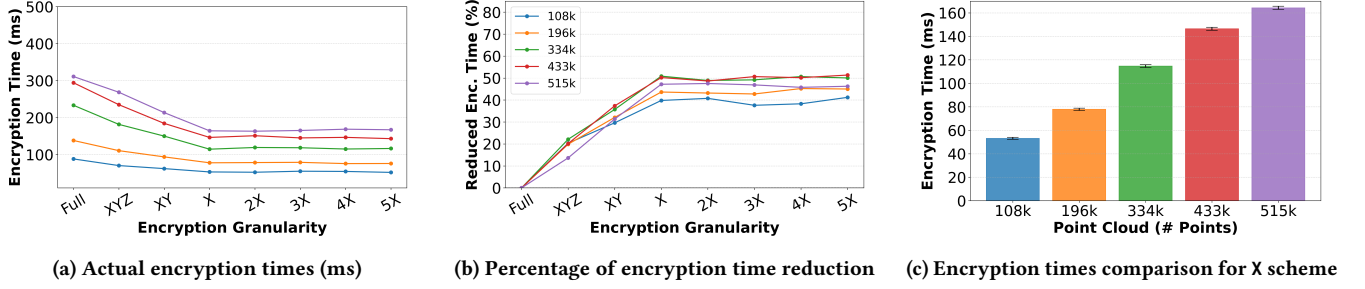


Figure 4: Evaluation of encryption times across various granularities and point cloud sizes.

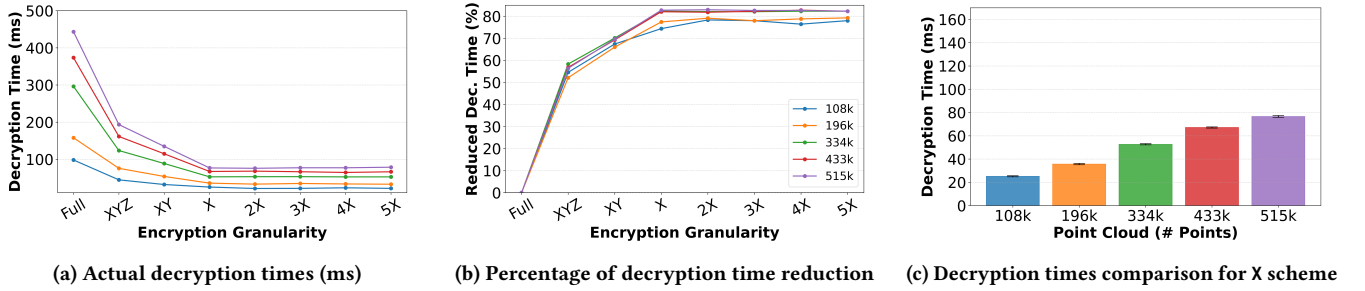


Figure 5: Evaluation of decryption times across various granularities and point cloud sizes.

in Fig. 6a. The XYZ scheme is omitted from discussion since zeroing all three coordinates collapses the point cloud to a single point—yielding complete obfuscation. In the XY case (Fig. 6b), zeroing two axes reduces the cloud to a line, eliminating all structural information and offering strong protection. Zeroing only X (Fig. 6c) produces a flattened projection; much of the scene’s semantics are lost (e.g., objects such as the chair become unrecognizable). In contrast, the 2X scheme (Fig. 6d), which zeroes every other x-coordinate, yields a mixed result: one half resembles the flattened projection seen in the X scheme, while the other half remains largely intact. This drastically weakens obfuscation, as significant portions of the scene remain visually interpretable. This limitation generalizes to any n th scheme. Next, we analyze the level of obfuscation achieved under each granularity using standard point cloud quality metrics.

Chamfer Distance (CD): Figure 7 reports the CD values for each encryption granularity. the XYZ scheme produces the largest CD, indicating maximal geometric deviation and therefore the strongest obfuscation. As we go to finer granularity—from XY to X—CD values drop accordingly, indicating reduced distortion and obfuscation. For coarser ones such as 2X through 5X, the CD approaches negligible levels, showing that these granularities provide minimal obfuscation. These findings show that meaningful obfuscation is achieved only when at least all X coordinates are removed.

Hausdorff Distance (HD): The HD trends in Fig. 7 mirror those of CD. The XYZ, XY, and X schemes yield the highest HD values—corresponding to the largest worst-case deviations and therefore the highest obfuscations—while coarser granularities (2X–5X) exhibit sharp declines, offering minimal obfuscation.

Overall, these observations indicate that encrypting at least all X coordinates is necessary to achieve meaningful obfuscation which

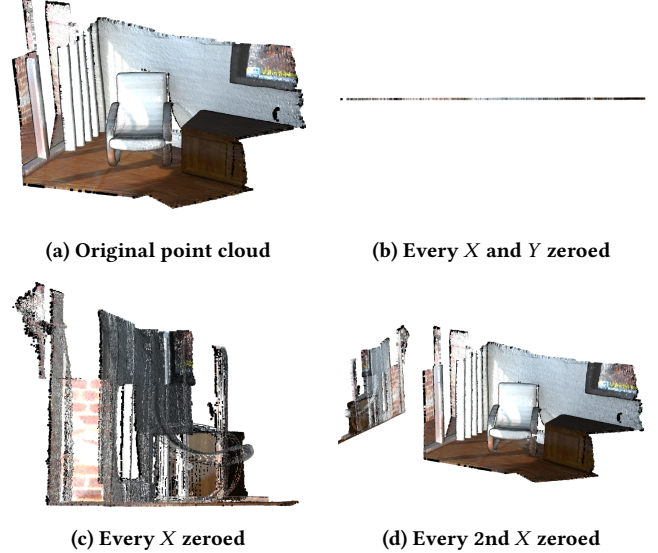


Figure 6: Visualization of point clouds with zeroed coordinates under different schemes.

still provides substantial computational gains. Moving to coarser granularities (e.g., 2X or n th X) offers negligible to no speedup, since runtime savings plateau, while significantly weakening obfuscation. Furthermore, an unauthorized user could attempt simple interpolation—such as averaging neighboring nonzero coordinates—to

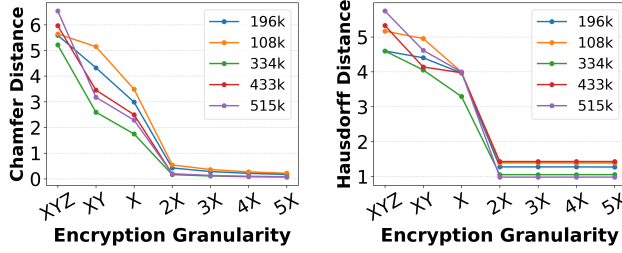


Figure 7: Quality evaluation metrics: higher is better.

partially reconstruct the missing geometry, reducing the security of coarser granularities even further.

4.2 Streaming Setup & Metrics

4.2.1 Setup:

Point cloud video dataset: To emulate a 60-second point cloud video at 24 FPS, we generated $24 \times 60 = 1440$ point cloud frames using the 108k-point model described in Sect. 4.1.1. This results in an approximate video bitrate of about 1 Gbit/s for our dataset. We then created four MPDs for our streaming experiments. One MPD was used for both HTTP-only and HTTPS streaming, listing the original, unencrypted point cloud frames. For HTTP-ABE, we prepared three additional MPDs—corresponding to the XYZ, XY, and X granularities—each referencing pre-encrypted frames generated using the respective selective-encryption scheme. We selected these three granularities because they provide meaningful visual obfuscation and significant computational benefits; beyond X, obfuscation becomes poor with no additional savings (Sect. 4.1). This setup enables a direct comparison across HTTP-only, HTTP-ABE (three schemes), and HTTPS streaming.

CloudLab setup: We perform our evaluations on the CloudLab testbed [9] using a simple five-node topology. One node hosts the origin server containing the point cloud content, a second node acts as a cache directly connected to the server, and the remaining three nodes function as client machines, each connected directly to the cache. Each client node runs eight independent streaming clients, yielding a total of 24 clients.

Each cache-client link provides approximately 9.4 Gbit/s. Given our emulated point cloud video bitrate of 1 Gbit/s per stream, each client node requires up to 8 Gbit/s of bandwidth, meaning 9.4 Gbit/s per link is sufficient to avoid contention on client-side paths. In contrast, we deliberately allow the server-cache link to experience pressure: it also operates at 9.4 Gbit/s, serving all 24 clients whose combined demand is roughly 24 Gbit/s. This creates a congested server-cache link, consistent with prior streaming studies [41, 42].

Apache HTTP server and Apache Traffic server: We use the Apache HTTP Server [2] on the origin server with TLS/SSL enabled to support HTTPS. Caching is provided by Apache Traffic Server (ATS) [3], which is configured using the remap plugin to forward all client requests to the origin. We evaluate two cache configurations: caching disabled (0 MB) and caching enabled with a 2000 MB cache size. For HTTPS experiments, ATS is configured to perform SSL

termination, enabling secure connections between the origin and the cache and between the cache and each client.

Streaming clients: On the client side, we run eight instances of the PC-Stream client on each of the three client nodes, totaling 24 clients. Each client uses a buffer size of 6, allowing six seconds of frames to be queued, which is also the initial startup buffer. For the HTTP-ABE experiments, we enable parallel download and decryption with a download queue size of 10. Client start times are scheduled using a Poisson distribution [24] with $\lambda = 5$, resulting in each client beginning its session approximately five seconds after the previous one on average.

4.2.2 Evaluation Metrics:

CPU load: We record CPU load on all nodes (origin server, cache, and client nodes) to compare performance across the HTTP-ABE granularities, HTTPS, and HTTP-only experiments. To do so, we use Linux’s `pidstat` [8] to monitor CPU utilization at a one-second sampling interval and collect CPU usage over the full duration of each experiment.

Hit Rate: We also compare the performance of the different approaches in terms of cache hit rates. We make use of ATS monitoring logs, which report the number of cache hits and misses during each experiment.

Rebuffering: On the client side, we use rebuffering as a metric to compare QoE across the different approaches. Rebuffering represents the time during which playback stalls because the client’s buffer is empty. We obtain rebuffering data from the PC-Stream client logs, which record stall duration for each frame. These per-frame values are accumulated to produce the total rebuffering time for each client session. We then average these totals across all clients and compute the rebuffering percentage relative to the full video duration (60 seconds) to assess overall performance.

4.3 HTTP vs HTTP-ABE vs HTTPS

The following evaluation assesses the performance of ABE-VVS using the end-to-end distribution pipeline using the setup and metrics defined in Sect. 4.2.

We analyze five streaming schemes: *HTTP-ONLY* (no security), three HTTP-based ABE-VVS configurations—*ABE-XYZ*, *ABE-XY*, and *ABE-X*—and *HTTPS*, which secures communication with TLS.

For each scheme, we conduct three experiments: one with caching disabled (0 MB) and two with a 2000 MB cache. The first 2000 MB run serves as a warm-up to populate the cache, and no metrics are collected during this phase. The second run is performed right after that, and only its results are used for evaluation. This warm-up process removes cache start-up effects and ensures fair comparison across all schemes.

4.3.1 CPU load: First, we discuss the average CPU load on the server, cache, and clients. Since each node on CloudLab has 32 cores, we sum the usage on all cores and plot the average usage throughout each streaming session. This period covers the start and end of all streaming sessions initiated by the 24 clients.

Server CPU load: Figure 8 (left) shows the average CPU load at the origin server. As expected, HTTPS incurs the highest CPU usage because the server must perform TLS encryption for every incoming request. In contrast, the ABE-based schemes operate on

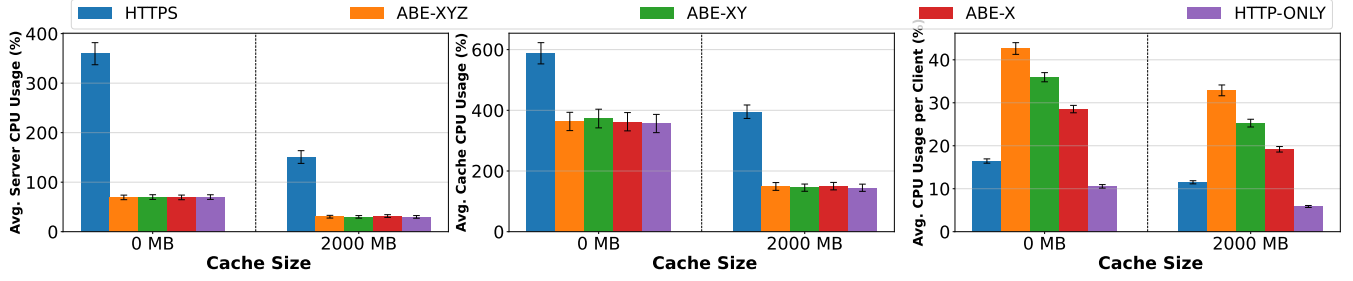


Figure 8: Average CPU usage; server (left), cache (middle) and per client (right).

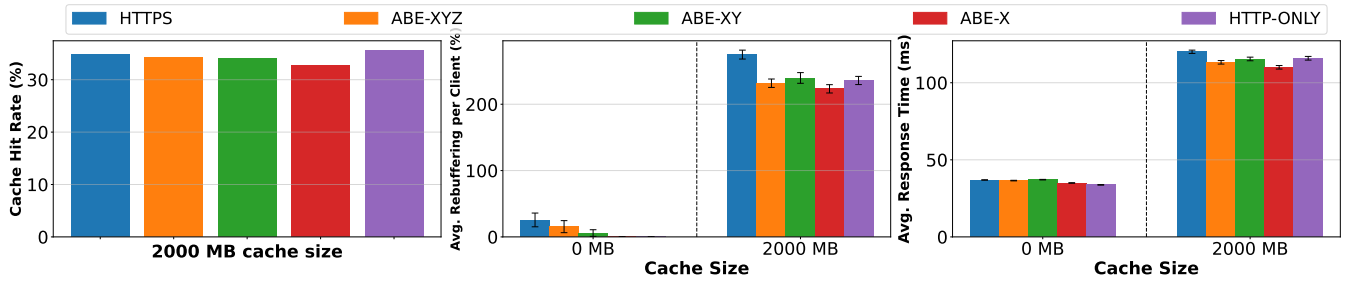


Figure 9: Cache hit rates (left), average rebuffering per client (middle) and average cache response time per request (right).

pre-encrypted segments—leveraging ABE’s ability to encrypt content once and distribute it securely to many users—thereby avoiding the repeated per-client encryption that TLS requires. Under the 0MB cache configuration, all HTTP-based ABE schemes—as well as the HTTP-only baseline—use approximately 80% less CPU than HTTPS. With a 2000MB cache, the overall CPU load decreases across all schemes due to the reduction in forwarded requests from the cache. However, the relative gap remains consistent, with HTTPS still requiring significantly more CPU and the other schemes maintaining roughly an 80% reduction in comparison.

Cache CPU load: For CPU usage at the cache, we observe a trend similar to that of the origin server. Figure 8 (middle) shows the average CPU load on the cache for both the 0 MB and 2000 MB configurations. HTTPS consistently exhibits the highest CPU usage because the cache must perform TLS operations both when fetching content from the server and when serving it to clients. For the latter case, this is also true even if the content is already cached. As expected, overall CPU usage is higher in the 0 MB configuration for all schemes, since every request must be forwarded to the origin server. In this case, the HTTP-ABE and HTTP-only schemes use, on average, 36–39% less CPU than HTTPS. With a 2000 MB cache, CPU usage decreases across all schemes due to fewer forwarded requests, but the relative difference widens: HTTP-ABE and HTTP-only reduce CPU consumption by roughly 63% compared to HTTPS.

Client CPU load: Finally, we examine CPU usage on the clients. For each experiment, we average the total CPU utilization across all three client nodes and report per-client usage in Fig. 8 (right). Among all schemes, the ABE configurations exhibit the highest client-side CPU load—most notably ABE-XYZ. This is expected:

client-side processing involves point cloud parsing, selective coordinate decryption, and reconstruction (Sect. 3.2), and the workload grows with the number of coordinates targeted for decryption.

With the 0 MB cache configuration, ABE-XY reduces CPU usage by about 16% compared to ABE-XYZ, while ABE-X reduces it by 33%. HTTPS requires 61% less CPU than ABE-XYZ, and HTTP-only uses 75% less, since it involves no decryption. With a 2000 MB cache, overall CPU usage decreases for all schemes, and the relative differences shift slightly: ABE-XY uses 23% less CPU than ABE-XYZ, ABE-X uses 41% less, HTTPS saves 65%, and HTTP-only saves 82%. Across both cache sizes, HTTP-only consistently consumes the least CPU because no security mechanism and hence no decryption runs on the client.

4.3.2 Hitrates: We also evaluate cache performance in terms of hit rates. Figure 9 (left) reports the hit rate percentages for the 2000 MB cache configuration across all schemes. The hit rate for the 0 MB/disable cache is always zero and is therefore omitted from analysis. All schemes achieve similar hit rates of roughly 33–35%, indicating that secure streaming has little impact on cache effectiveness compared to HTTP-only. This includes the ABE schemes, even though the pre-encrypted frames are slightly larger in size.

4.3.3 Rebuffering: Figure 9 (middle) reports client-side QoE in terms of rebuffing. Rebuffing is expressed as a percentage of the total point cloud video duration (60 seconds).

For the 0 MB cache configuration, we observe the expected behavior: HTTPS experiences the highest rebuffing (about 25%), followed by ABE-XYZ at roughly 15% and ABE-XY at around 6%. For ABE-X and HTTP-only, no rebuffing is observed. These results indicate that ABE-X is the lightest selective-encryption scheme—it

provides reasonable obfuscation (Sect. 4.1.4) while adding minimal latency, resulting in no client-side QoE degradation. ABE-XY incurs only minor rebuffering, ABE-XYZ somewhat more, while HTTPS performs the worst, demonstrating that our ABE-based approach introduces substantially lower overhead than HTTPS.

Under the 2000 MB cache configuration, however, we observe an unexpected trend: rebuffering increases dramatically compared to the 0 MB case. While larger caches usually reduce stalls due to higher hit rates—as shown in prior studies [25, 41, 42]—our experiments show rebuffering of 220–240% for all ABE and HTTP-only schemes, and about 275% for HTTPS. We also do not see the expected pattern where lighter ABE schemes (or HTTP-only) yield lower rebuffering. Upon investigation, we found that this anomaly is caused by increased cache response times under the 2000 MB configuration, which we discuss in the following subsection.

4.3.4 Cache response time: To understand the unexpectedly high rebuffering observed with the 2000 MB cache configuration, we examined the internal cache logs and analyzed per-request response times. Figure 9 (right) reports the average cache response time per request for all schemes under both the 0 MB and 2000 MB configurations. We found that cache response times with the 2000 MB cache were significantly higher than with the 0 MB configuration. Specifically, with 0 MB, average response times across all schemes ranged between 34–37 ms. In the case of a 2000 MB cache, they increased to 110–120 ms—roughly a threefold increase.

This behavior is due to the cache’s slower disk read/write operations. In the 0 MB configuration (or in cases of cache misses), the cache simply fetches content from the origin and forwards it directly from memory. In contrast, with the 2000 MB cache, the cache must first locate and then read each frame from disk before serving it to the client. These disk operations substantially increase latency, and the effect is amplified in our per-frame streaming setup, where at least 12 clients are simultaneously requesting point cloud frames at a rate of 24 FPS.

With a faster cache, this bottleneck would be largely eliminated, and we would expect trends similar to those observed in the 0 MB configuration, where scheme-dependent differences were clearly visible. However, in our 2000 MB case, the elevated cache response times dominate overall latency and lead to the large rebuffering values seen earlier.

We also note that client CPU usage at 2000 MB is lower than in the 0 MB case (Fig. 8, right). This is because higher latency and frequent stalls reduce the rate at which clients can decrypt and process frames, thereby lowering their average CPU load.

5 Discussion

In this work, we evaluated ABE-VVS in an on-demand streaming setting. Because ABE supports point-to-multipoint distribution, all point cloud frames were pre-encrypted and stored in the origin server in encrypted form, meaning that no per-request encryption was required during streaming for the ABE schemes. In contrast, HTTPS relies on point-to-point TLS encryption, so the origin server must perform encryption for every incoming request.

For live streaming scenarios, ABE encryption would need to be performed at the origin server as new point cloud frames are generated. However, unlike HTTPS, ABE would still avoid repeated

encryption of identical content for multiple viewers. As discussed in Sect. 4.1, our evaluation of selective coordinate encryption shows that encrypting only the X coordinates reduces encryption time by up to 50% compared to full-frame encryption. These savings suggest that applying ABE-VVS to live volumetric streaming could yield promising performance benefits—an interesting direction for future exploration.

6 Conclusions

In this work, we presented ABE-VVS which enables selective coordinate encryption for protecting point cloud video streaming using Attribute-Based Encryption (ABE). By encrypting only targeted subsets of X, Y, Z coordinates rather than entire frames, our method lowers computational cost while still producing strong obfuscation that prevents meaningful unauthorized viewing. Our results show that encrypting only the X coordinate offers substantial obfuscation with up to 50% decreased encryption time and up to 80% decreased decryption time compared to full-frame encryption.

Our work is novel in integrating and evaluating security in the point cloud streaming pipeline. In our evaluations, we compared three ABE granularities (XYZ, XY, X) against HTTPS and HTTP-only baselines on a CloudLab deployment. The results show that our ABE schemes significantly reduce CPU load at the server and cache by as much as 80% and 63%, respectively, while maintaining hit rates comparable to unsecured HTTP-only streaming. On the client-side ABE-XYZ and ABE-XY incur lower rebuffering than HTTPS, while ABE-X achieves rebuffering-free playback similar to HTTP-only. Although our ABE schemes increased the CPU usage of the client, the added overhead remains manageable.

This study focused on per-frame delivery and a single point cloud quality level. Future work will incorporate segment-based delivery and multi-bitrate support for point clouds to evaluate adaptive bitrate (ABR) streaming conditions.

References

- [1] M.H. Annaby, M.E. Mahmoud, H.A. Abdusalam, H.A. Ayad, and M.A. Rushdi. 2024. On 3D encryption schemes based on chaotic permutations and rotations with geometric stability. *Optik* 300 (2024), 171680. doi:10.1016/j.ijleo.2024.171680
- [2] Apache. 2024. *Apache HTTP Server Project*. Retrieved 2024 from <https://httpd.apache.org/>
- [3] Apache. 2024. *Apache Traffic Server*. Retrieved 2024 from <https://trafficserver.apache.org/>
- [4] John Bethencourt. 2011. *Using the cpabe Toolkit*. Retrieved 2024 from <https://acsc.cs.utexas.edu/cpabe/tutorial.html>
- [5] John Bethencourt, Amit Sahai, and Brent Waters. 2007. Ciphertext-Policy Attribute-Based Encryption. In *2007 IEEE Symposium on Security and Privacy (SP '07)*. 321–334. doi:10.1109/SP.2007.11
- [6] Yumeko Chujo, Yusuke Tagashira, Yukiko Harada, Kenji Kanai, and Jiro Katto. 2024. Perceptual Quality Driven Point Cloud Compression for 6DoF 3D Point Cloud Streaming. In *2024 International Symposium on Multimedia (ISM)*. 154–157. doi:10.1109/ISM63611.2024.00034
- [7] Matthias De Fré, Jeroen van der Hooft, Tim Wauters, and Filip De Turck. 2024. Scalable MDC-Based Volumetric Video Delivery for Real-Time One-to-Many WebRTC Conferencing. In *Proceedings of the 15th ACM Multimedia Systems Conference (Bari, Italy) (MMSys '24)*. Association for Computing Machinery, New York, NY, USA. 121–131. doi:10.1145/3625468.3647617
- [8] die.net. 2024. *pidstat - Report statistics for Linux tasks*. <https://linux.die.net/man/1/pidstat>
- [9] Dmitry Duplyakin, Robert Ricci, Aleksander Maricq, Gary Wong, Jonathon Duerig, Eric Eide, Leigh Stoller, Mike Hibler, David Johnson, Kirk Webb, Aditya Akella, Kuangching Wang, Glenn Ricart, Larry Landweber, Chip Elliott, Michael Zink, Emmanuel Cecchet, Snigdhaswin Kar, and Prabodh Mishra. 2019. The Design and Operation of CloudLab. In *2019 USENIX Annual Technical Conference (USENIX ATC '19)*. USENIX Association, Renton, WA, 1–14. <https://www.usenix.org/conference/atc19/presentation/duplyakin>

//www.usenix.org/conference/atc19/presentation/duplyakin

[10] Serhan Gül, Dimitri Podborski, Thomas Buchholz, Thomas Schierl, and Cornelius Hellge. 2020. Low-latency cloud-based volumetric video streaming using head motion prediction. In *Proceedings of the 30th ACM Workshop on Network and Operating Systems Support for Digital Audio and Video* (Istanbul, Turkey) (NOSS-DAV '20). Association for Computing Machinery, New York, NY, USA, 27–33. doi:10.1145/3386290.3396933

[11] Simon N. B. Gunkel, Rick Hindriks, Karim M. El Assal, Hans M. Stokking, Sylvie Dijkstra-Soudarissanane, Frank ter Haar, and Omar Niamut. 2021. VRComm: an end-to-end web system for real-time photorealistic social VR communication. In *Proceedings of the 12th ACM Multimedia Systems Conference* (Istanbul, Turkey) (MMSys '21). Association for Computing Machinery, New York, NY, USA, 65–79. doi:10.1145/3458305.3459595

[12] Hadi Heidarirad and Mea Wang. 2025. VV-DASH: A Framework for Volumetric Video DASH Streaming. In *Proceedings of the 16th ACM Multimedia Systems Conference* (Stellenbosch, South Africa) (MMSys '25). Association for Computing Machinery, New York, NY, USA, 256–262. doi:10.1145/3712676.3718339

[13] Mohammad Hosseini and Christian Timmerer. 2018. Dynamic Adaptive Point Cloud Streaming. In *Proceedings of the 23rd Packet Video Workshop* (MMSys '18). ACM, 25–30. doi:10.1145/3210424.3210429

[14] Gangyang Hou, Bo Ou, Fei Peng, and Min Long. 2025. A Traitor Tracing and Access Control Method for Encrypted 3D Models Based on CP-ABE and Fair Watermark. *IEEE Signal Processing Letters* 32 (2025), 696–700. doi:10.1109/LSP.2024.3522860

[15] Tzu-Kuan Hung, I-Chun Huang, Samuel Rhys Cox, Wei Tsang Ooi, and Cheng-Hsin Hsu. 2022. Error Concealment of Dynamic 3D Point Cloud Streaming. In *Proceedings of the 30th ACM International Conference on Multimedia* (Lisboa, Portugal) (MM '22). Association for Computing Machinery, New York, NY, USA, 3134–3142. doi:10.1145/3503161.3548384

[16] Jong-Beom Jeong, Soonbin Lee, Dongmin Jang, and Eun-Seok Ryu. 2019. Towards 3DoF 360 Video Streaming System for Immersive Media. *IEEE Access* 7 (2019), 136399–136408. doi:10.1109/ACCESS.2019.2942771

[17] Xin Jin, Zhaoxing Wu, Chenggen Song, Chunwei Zhang, and Xiaodong Li. 2016. 3D Point Cloud Encryption Through Chaotic Mapping. Vol. 9916. 119–129. doi:10.1007/978-3-319-48890-5_12

[18] Yili Jin, Kaiyuan Hu, Junhua Liu, Fangxin Wang, and Xue Liu. 2024. From Capture to Display: A Survey on Volumetric Video. arXiv:2309.05658 [cs.MM] https://arxiv.org/abs/2309.05658

[19] Alireza Jolfaei, Xin-Wen Wu, and Vallipuram Muthukumarasamy. 2015. A 3D Object Encryption Scheme Which Maintains Dimensional and Spatial Stability. *IEEE Transactions on Information Forensics and Security* 10, 2 (2015), 409–422. doi:10.1109/TIFS.2014.2378146

[20] Xusheng Li, Jinqing Li, Xiaoqiang Di, Hongmei Guan, Mingao Zhang, Mengli Gao, and Makram Ibrahim. 2024. 3D point cloud encryption algorithm based on hybrid key and spatial maintenance. *Journal of Information Security and Applications* 87 (2024), 103896. doi:10.1016/j.jisa.2024.103896

[21] Jianqiang Liu, Jian Yao, Jingmin Tu, and Junhao Cheng. 2019. Data-Adaptive Packing Method for Compression of Dynamic Point Cloud Sequences. In *2019 IEEE International Conference on Multimedia and Expo (ICME)*. 904–909. doi:10.1109/ICME.2019.000160

[22] Junhua Liu, Boxiang Zhu, Fangxin Wang, Yili Jin, Wenyi Zhang, Zihan Xu, and Shuguang Cui. 2023. CaV3: Cache-assisted Viewport Adaptive Volumetric Video Streaming. In *2023 IEEE Conference Virtual Reality and 3D User Interfaces (VR)*. 173–183. doi:10.1109/VR5154.2023.00033

[23] Zhaoyang Lyu, Zhipeng Kong, Xudong Xu, Liang Pan, and Dahu Lin. 2021. A Conditional Point Diffusion-Refinement Paradigm for 3D Point Cloud Completion. *CoRR* abs/2112.03530 (2021). arXiv:2112.03530 https://arxiv.org/abs/2112.03530

[24] NumPy. 2024. *numpy.random.poisson*. Retrieved 2024 from https://numpy.org/doc/stable/reference/random/generated/numpy.random.poisson.html

[25] Claudiu Olteanu, Mihai Bucicou, and Marius Popa. 2016. SStream: An Infrastructure for Streaming Multimedia Content Efficiently and Securely in a Heterogeneous Environment. In *Exploring Services Science*, Theodor Borangiu, Monica Dragoicea, and Henriqueta Nóvoa (Eds.). Springer International Publishing, Cham, 343–354.

[26] open3d.org. 2025. *Dataset*. https://www.open3d.org/docs/release/tutorial/data/index.html

[27] Jounsup Park, Mingyuan Wu, Kuan-Ying Lee, Bo Chen, Klara Nahrstedt, Michael Zink, and Ramesh Sitaraman. 2020. SEAWARE: Semantic Aware View Prediction System for 360-degree Video Streaming. In *2020 IEEE International Symposium on Multimedia (ISM)*. 57–64. doi:10.1109/ISM50200.00016

[28] Cédric Portaneri, Pierre Alliez, Michael Hemmer, Lukas Birklein, and Elmar Schoemer. 2019. Cost-driven framework for progressive compression of textured meshes. In *Proceedings of the 10th ACM Multimedia Systems Conference* (Amherst, Massachusetts) (MMSys '19). Association for Computing Machinery, New York, NY, USA, 175–188. doi:10.1145/3304109.3306225

[29] David Reddick, F. Alex Feltus, and Susmit Shannigrahi. 2022. Case Study of Attribute Based Access Control for Genomics Data Using Named Data Networking. In *IEEE CCNC*.

[30] David Reddick, Justin Presley, F. Alex Feltus, and Susmit Shannigrahi. 2022. AABAC – Automated Attribute Based Access Control for Genomics Data. arXiv:2204.04591 [cs.CR] https://arxiv.org/abs/2204.04591

[31] David Reddick, Justin Presley, Frank Alex Feltus, and Susmit Shannigrahi. 2022. WiP: AABAC-Automated Attribute Based Access Control for Genomics Data. In *Proceedings of the 27th ACM on Symposium on Access Control Models and Technologies*. 217–222.

[32] David Eugene Reddick. 2021. *Design of an NDN-Based Data Distribution Infrastructure for Genomics Data Secured with a Novel Ledger Access System Founded on Attribute-Based Encryption*. Master's thesis. Tennessee Technological University.

[33] Eric Rescorla. 2018. The Transport Layer Security (TLS) Protocol Version 1.3. RFC 8446. doi:10.17487/RFC8446

[34] Iraj Sodagar. 2011. The mpeg-dash standard for multimedia streaming over the internet. *IEEE multimedia* 18, 4 (2011), 62–67.

[35] Jan-Philipp Stauffert, Florian Niebling, and Marc Erich Latoschik. 2020. Latency and Cybersickness: Impact, Causes, and Measures. A Review. *Frontiers in Virtual Reality* Volume 1 - 2020 (2020). doi:10.3389/fvrir.2020.582204

[36] Junshu Tang, Zhijun Gong, Ran Yi, Yuan Xie, and Lizhuang Ma. 2022. LAKe-Net: Topology-Aware Point Cloud Completion by Localizing Aligned Keypoints. In *2022 IEEE/CVF Conference on Computer Vision and Pattern Recognition (CVPR)*. 1716–1725. doi:10.1109/CVPR52688.2022.00177

[37] Zhongze Tang, Xianglong Feng, Yi Xie, Huy Phan, Tian Guo, Bo Yuan, and Sheng Wei. 2020. VVSec: Securing Volumetric Video Streaming via Benign Use of Adversarial Perturbation. In *Proceedings of the 28th ACM International Conference on Multimedia* (Seattle, WA, USA) (MM '20). Association for Computing Machinery, New York, NY, USA, 3614–3623. doi:10.1145/3394171.3413639

[38] Greg Turk. 2025. *The PLY Polygon File Format*. https://web.archive.org/web/20161204152348/http://www.dcs.ed.ac.uk/teaching/cs4/www/graphics/Web/ply.html

[39] USAVPS. 2023. *CDN Basic – How CDNs handle encrypted content*. Retrieved 2024 from https://usavps.com/blog/17594/

[40] Mohammad Waqas Usmani, Susmit Shannigrahi, and Michael Zink. 2025. Lightweight DRM for Volumetric Point Clouds through Attribute-Based Selective Coordinate Encryption. In *Proceedings of the Twenty-Sixth International Symposium on Theory, Algorithmic Foundations, and Protocol Design for Mobile Networks and Mobile Computing* (Rice University, Houston, TX, USA) (Mobi-Hoc '25). Association for Computing Machinery, New York, NY, USA, 456–461. doi:10.1145/3704413.3765298

[41] Mohammad Waqas Usmani, Susmit Shannigrahi, and Michael Zink. 2025. Secure the Stream, Not the Hosts: Attribute-Based Encryption for DRM Enabled Video Streaming. In *Proceedings of the 16th ACM Multimedia Systems Conference* (Stellenbosch, South Africa) (MMSys '25). Association for Computing Machinery, New York, NY, USA, 190–200. doi:10.1145/3712676.3714450

[42] Mohammad Waqas Usmani, Susmit Shannigrahi, and Michael Zink. 2025. Securing Immersive 360 Video Streams through Attribute-Based Selective Encryption. arXiv:2505.04466 [cs.MM] https://arxiv.org/abs/2505.04466

[43] Mohammad Waqas Usmani, Sankalpa Timilsina, Michael Zink, and Susmit Shannigrahi. 2025. Secure AI-Driven Super-Resolution for Real-Time Mixed Reality Applications. arXiv:2512.15823 [cs.CR] https://arxiv.org/abs/2512.15823

[44] Jeroen van der Hooft, Maria Torres Vega, Christian Timmerer, Ali C. Begen, Filip De Turck, and Raimund Schatz. 2020. Objective and Subjective QoE Evaluation for Adaptive Point Cloud Streaming. In *2020 Twelfth International Conference on Quality of Multimedia Experience (QoMEX)*. 1–6. doi:10.1109/QoMEX48832.2020.9123081

[45] Jeroen van der Hooft, Tim Wauters, Filip De Turck, Christian Timmerer, and Hermann Hellwagner. 2019. Towards 6DoF HTTP Adaptive Streaming Through Point Cloud Compression. In *Proceedings of the 27th ACM International Conference on Multimedia* (Nice, France) (MM '19). Association for Computing Machinery, New York, NY, USA, 2405–2413. doi:10.1145/3343031.3350917

[46] Rui Xin, Shihuan Lin, and Xiaowei Yang. 2023. Quantifying User Password Exposure to Third-Party CDNs. In *Passive and Active Measurement: 24th International Conference, PAM 2023, Virtual Event, March 21–23, 2023, Proceedings*. Springer-Verlag, Berlin, Heidelberg, 652–668. doi:10.1007/978-3-031-28486-1_27

[47] Anlan Zhang, Chengdong Wang, Bo Han, and Feng Qian. 2022. YuZu: Neural-Enhanced Volumetric Video Streaming. In *19th USENIX Symposium on Networked Systems Design and Implementation (NSDI 22)*. USENIX Association, Renton, WA, 137–154. https://www.usenix.org/conference/nsdi22/presentation/zhang-anlan